Direct photodegradation of 36 organic micropollutants under simulated solar radiation: Comparison with free-water surface constructed wetland and influence of chemical structure

Baptiste Mathon, Martial Ferréol, Marina Coquery, J.M. Choubert, Jean-Marc Chovelon, Cecile Miege

Direct photodegradation of 36 organic micropollutants under simulated solar radiation: comparison with free-water surface constructed wetland and influence of chemical structure

***[1-2]Baptiste Mathon, [2]Martial Ferreol, [2]Marina Coquery, M., [1]Jean-Marc Choubert, [3]Jean-Marc Chovelon, [2]Cécile Miège.**

[1]INRAE, UR REVERSAAL, 5 rue de la Doua, CS 20244, F-69625 Villeurbanne, France
[2]INRAE, UR RiverLy, F-69625 Villeurbanne, France
[3]Université Claude Bernard Lyon 1, CNRS UMR 5256, IRCELYON, F-69626, 2 avenue Albert-Einstein, Villeurbanne, France
*Corresponding author, baptiste.mathon@inrae.fr

Citation: Mathon, B., Ferreol, M., Coquery, M., Choubert, J.M., Chovelon, J.M., Miège, C. (2021). Direct photodegradation of 36 organic micropollutants under simulated solar radiation: Comparison with free-water surface constructed wetland and influence of chemical structure, Journal of Hazardous Materials, 407, 124801,

Abstract

Micropollutants such as pharmaceuticals and pesticides are still found in treated municipal effluent and are discharged into the natural environment. Natural direct photodegradation may be one pathway for removing these micropollutants in treatment processes such as free-water surface constructed wetlands (CW). This work was set out to evaluate the half-life ($t_{1/2}$) of direct photodegradation of 36 micropollutants under controlled conditions of light exposure close to solar radiation. The results allowed to classify the micropollutants into three groups (fast, medium and slow). Seven micropollutants were classified in the fast group with $t_{1/2}$ between 0.05 h and 0.79 h, 24 in the medium group with $t_{1/2}$ between 5.3 h and 49.7 h, and five in the slow group with $t_{1/2}$ between 56 h and 118 h. The $t_{1/2}$ values obtained in laboratory were compared with those from a CW receiving treated wastewater. Correction factors were calculated to adjust the in situ data for the light intensity in laboratory and improved the correspondence especially for the micropollutants of the fast and medium groups. Finally, an innovative method based on statistical tests highlighted the chemical functions characteristic of micropollutants sensitive to photodegradation (OH–C=O, C=N–O–, =N–OH, –CH=N, –O–P=O, –C=C–) and with low sensitivity (–O–R, –Cl).

Keywords: direct photodegradation, light intensity, chemical functions, organic micropollutant, free-water surface constructed wetland

1. Introduction

Over the past 20 years, many studies have demonstrated the presence of micropollutants in wastewater treatment plants (WWTPs). Many micropollutants persist in treated wastewater, such as pesticides, pharmaceuticals, hormones, etc. (Miège et al., 2009; Verlicchi et al., 2012; Luo et al., 2014; Tran et al., 2018). These micropollutants are quantified at concentrations of the order of $ng.L^{-1}$ for hormones (e.g. estrone) to $\mu g.L^{-1}$ for pharmaceuticals (e.g. diclofenac, ibuprofen, atenolol, carbamazepine) and pesticides (e.g. diuron, diazinon) (Miège et al., 2009; Verlicchi et al., 2012; Luo et al., 2014; Ben et al., 2018). Treated wastewaters are discharged into the natural environment, and many pharmaceuticals and pesticides have been quantified in rivers (Luo et al., 2014; Gonzalez-Rey et al., 2015). These micropollutants can prove toxic at environmental concentration levels and produce a wide range of responses in non-target organisms (Fent et al., 2006; Brodin et al., 2013; Pal et al., 2006).

Current European legislation, and specifically the Water Framework Directive (WFD, 2000/60/EC, European Commission, 2000), does not impose a discharge limit on the concentrations of micropollutants in liquid effluents from WWTPs. However, the WFD and French regulations specify that the release of priority substances of the Watch List must be reduced or even stopped (Decision 2015/495/EC, European Commission, 2015). To meet these reduction objectives, many studies have sought to identify effective processes for eliminating micropollutants in wastewater treatment plants (Grandclément et al., 2017; Reyes Contreras et al., 2019; Silva et al., 2019). Recent literature further reports that pharmaceuticals and pesticides can also be eliminated by natural photodegradation (Burrows et al., 2002; Fatta-Kassinos et al., 2011; Challis et al., 2014), specifically as polishing treatment complementary to secondary treatment in the context of a free-water surface constructed wetland (CW) (Mathon et al., 2019). The photodegradation mechanisms take two different pathways. The first, direct photolysis, occurs by absorption of UV rays by the micropollutant. The second, indirect photolysis, is possible in the presence of photosensitizers (nitrates, nitrites, dissolved organic matters (DOM), etc.), which promote the generation of reactive species ($^1O_2$, $OH^\bullet$ and $CO_3^{-\bullet}$ radicals and the excited triplet state $^3DOM^*$), leading to the degradation of the micropollutant (Zepp, 1987).

A photochemical reaction occurs when a micropollutant first absorbs a photon leading to an electronically excited state. Then during the deactivation processes, photochemical reactions can take place from the lowest excited states whose lifetimes is sufficiently long (Braun et al., 1986).

To date, most micropollutant photodegradation studies have been carried out under controlled laboratory conditions with light exposure that differs from solar radiation (monochromatic light, too-high intensity, etc.), which is not satisfying as such conditions are too far from real conditions (Mathon et al., 2016). To be as close as possible to natural photodegradation experiments in the aquatic environment, Challis et al. (2014) proposed specific recommendations such as the use of light source

more close to sunlight intensity and wavelength range, a pH close to 7 and the absence of organic solvent in the spiked solutions.

The rate of a micropollutant photodegradation is generally characterized by a kinetic constant (k) or a half-life ($t_{1/2}$). The mechanisms of direct photodegradation are influenced by the environmental conditions and the nature of the micropollutant. However, the conditions of exposure, in particular the light intensity, the exposure time and the geometry of the photoreactors, are usually poorly documented in the literature, when they are, they usually differ from one author to another. As a result, the $t_{1/2}$ values determined for each micropollutant vary widely and are difficult to compare (Challis et al., 2014).

To enable a more rigorous comparison, Mathon et al. (2019) assessed *in situ* the photodegradability under solar radiation of 23 micropollutants in the context of a CW (Marguerittes, France). This study demonstrated that direct photodegradation was the predominant elimination pathway in that context.

In a same way it is difficult to relate the nature (chemical structure and intrinsic properties) of a micropollutant to its photodegradability based on data from the literature. Many publications concern the study of QSARs (quantitative structure-activity relationships), for predicting the behavior of organic micropollutants such as dissolution, volatilization, biodegradation, and adsorption with molecular intrinsic descriptors that need to be previously modeled and calculated (Mamy et al., 2015). Currently, such QSARs mainly use energy transitions (E_{LUMO}, E_{HOMO}) to predict photodegradation. In addition to such models, it would be interesting to test the influence of other descriptors, more easily available, such as physico-chemical properties or chemical structure characteristics (i.e., molecular weight, quantum yield, log K_{ow}, pKa, water solubility, functional groups and covalent bonds) to improve the prediction of micropollutant photodegradability .

Here, we present a controlled laboratory experiment of the direct photodegradation of 36 micropollutants with a wide range physico-chemical properties (molecular weight, quantum yield, log K_{ow}, etc.). The objective of this study was to evaluate the half-lives ($t_{1/2}$) and the kinetic constants of direct micropollutants photodegradation (k) under controlled conditions of light exposure close to those of solar radiation. The $t_{1/2}$ values for direct photodegradation measured under controlled conditions were compared with the $t_{1/2}$ values measured under real conditions (also focused on direct photodegradation) for the same micropollutants studied *in situ* in Mathon et al. (2019). This comparison also aimed to determine the best method for comparing results obtained under different conditions. Finally, statistical tests enabled to explore the relationships between the $t_{1/2}$ and the physico-chemical properties and structures of the micropollutants for predicting their direct photodegradation.

2. Materials and methods

2.1. Selection of micropollutants

A list of 36 micropollutants was drawn up (Table 1) for their well-known toxic effects on aquatic organisms and human health, their high occurrence in secondary treated wastewaters (Miège et al., 2009), and because they represented a wide range of physico-chemical properties, including photodegradation potential (i.e. molecular weight, quantum yield, log K_{ow}, water solubility, pKa).

112 *Table 1. The 36 micropollutants selected, their main physico-chemical characteristics and the limits of quantification in water.*

Micropollutant	**Abbreviation**	**Molecular weight ($g.mol^{-1}$)**	**Chemical formula**	**Family**	**Quantum yield Φ**	**Log K_{ow}**	**Solubility in water (25°C) (mg/L)**	**pK_a**	**Limit of quantification ($ng.L^{-1}$)**
Acebutolol	ACE	336.43	C18H28N2O4	Beta blockers	$6.0.10^{-7}$	1.71	259	9.4	0.2
Acetylsulfamethoxazole	ASUL	295.07	C12H13N3O4S	Metabolites	P.I.	1.21	1216	P.I.	0.2
Fenofibric acid	AFENO	318.75	C17H15ClO4	Metabolites	$2.0.10^{-4}$	4	9	P.I.	1
Alprazolam	ALP	308.77	C17H13ClN4	Anti-inflammatories	$3.4.10^{-6}$	2.12	40	P.I.	0.2
Amitriptyline	AMI	277.40	C20H23N	Anti-inflammatories	$3.0.10^{-3}$	4.92	10	9.4	1
Atenolol	ATE	266.34	C14H22N2O3	Beta blockers	$3.6.10^{-2}$	0.16	$1.33.10^{4}$	9.6	0.2
Atrazine	ATZ	215.68	C8H14ClN5	Pesticides	$1.0.10^{-4}$	2.61	35	P.I.	0.1
Azithromycin	AZI	748.98	C38H72N2O12	Antibiotics	P.I.	2.44	<1000	9.57	5
Carbamazepine	CBZ	236.27	C15H12N2O	Anti-depressants	$3.1.10^{-4}$	2.45	18	P.I.	0.2
Clarithromycin	CLA	747.95	C38H69NO13	Antibiotics	$5.0.10^{-4}$	3.16	0.33	8.99	1
Clindamycin	CLIN	424.98	C18H33ClN2O5S	Antibiotics	$3.0.10^{-4}$	2.16	31	P.I.	0.4
Cyclophosphamide	CYC	261.09	C7H15Cl2N2O2P	Anticancer	$4.0.10^{-4}$	0.63	$1\text{-}5.10^{4}$	P.I.	0.2
Diazepam	DIAZ	284.74	C16H13ClN2O	Anti-depressants	$4.3.10^{-6}$	2.82	50	3.4	0.2
Diclofenac	DICLO	296.15	C14H11Cl2NO2	Anti-inflammatories	$1.3.10^{-3}$	4.51	2	4.15	0.4
Dimethoate	DIM	229.26	C5H12NO3PS2	Pesticides	$5.0.10^{-5}$	0.78	$2.5.10^{4}$	P.I.	0.2
Diuron	DIU	233.09	C9H10Cl2N2O	Pesticides	$1.7.10^{-4}$	2.68	49	13.55	0.1
Erythromycin	ERY	733.93	C37H67NO13	Antibiotics	$4.0.10^{-4}$	3.06	2000	8.88	1
Fluoxetine	FLUOX	309.33	C17H18F3NO	Anti-depressants	P.I.	4.5	5.10^{4}	P.I.	4
Imidacloprid	IMI	255.66	C9H10ClN5O2	Pesticides	$8.6.10^{-4}$	0.57	610	P.I.	0.4
Isoproturon	ISO	206.28	C12H18N2O	Pesticides	$2.0.10^{-3}$	2.87	70	P.I.	0.1
Ketoprofen	KETO	254.28	C16H14O3	Anti-inflammatories	$1.0.10^{-3}$	3.12	51	4.45	0.2
Metoprolol	MET	267.36	C15H25NO3	Beta blockers	$2.0.10^{-2}$	1.88	$1.69.10^{4}$	P.I.	0.1
Metronidazole	METRO	171.15	C6H9N3O3	Antibiotics	$4.2.10^{-5}$	-0.02	9500	2.38	0.4
Nordiazepam	NORD	270.71	C15H11ClN2O	Anti-depressants	$1.7.10^{-6}$	2.93	9	P.I.	0.1
Norfluoxetine	NORF	295.3	C16H16F3NO	Metabolites	P.I.	3.8	9.15	P.I.	1
Ofloxacine	OFLO	361.37	C18H20FN3O4	Antibiotics	$3.0.10^{-3}$	-0.39	$2.8.10^{4}$	P.I.	2
Oxazepam	OXA	286.71	C15H11ClN2O2	Anti-depressants	$8.8.10^{-6}$	2.24	179	P.I.	0.2
Paracetamol	PARA	151.16	C8H9NO2	Anti-inflammatories	$4.6.10^{-2}$	0.46	$1.4.\ 10^{4}$	9.38	1
Pirimicarb	PIRI	238.29	C11H18N4O2	Pesticides	P.I.	1.4	970	P.I.	0.2
Propranolol	PROP	259.34	C16H21NO2	Beta blockers	$2.2.10^{-5}$	3.48	62	9.42	0.1
Salbutamol	SAL	239.31	C13H21NO3	Bronchodilators	$6.0.10^{-2}$	0.64	$1.4.\ 10^{4}$	10.3	0.4
Simazine	SIM	201.66	C7H12ClN5	Pesticides	$6.2.10^{-2}$	2.18	6	1.62	0.1
Sotalol	SOT	272.36	C12H20N2O3S	Beta blockers	$5.0.10^{-3}$	0.24	5510	P.I.	0.4
Sulfamethoxazole	SULFA	253.28	C10H11N3O3S	Antibiotics	$3.0.10^{-4}$	0.89	610	P.I.	0.2
Theophylline	THEO	180.16	C7H8N4O2	Anti-inflammatories	$8.0.10^{-6}$	-0.02	7360	8.81	1
Trimethoprime	TRIM	290.32	C14H18N4O3	Antibiotics	$3.0.10^{-5}$	0.91	400	6.6	0.2

113

2.2. Direct photodegradation experiments

For a better match with *in situ* photodegradation studies, we opted to work with a lamp simulating the solar radiation. We therefore selected an Atlas® suntest as the source of radiation which consists of a test chamber with a surface area of 560 cm^2 irradiated by a xenon arc lamp (power 500 watts), with a constant light dose of 765 Wm^{-2} in a wavelength range of 300–800 nm. In addition, the device comprised a cooling plate equipped with a circulation cryostat limiting as much as possible the rise in temperature in the test chamber. Agitation was provided by a magnetic stirrer placed under the cooling plate.

The reactor consisted of 500 mL of MilliQ LC-Pak ultrapure water in a quartz flask. A spiked solution containing the 36 micropollutants studied was added to the quartz flasks to obtain a concentration of 10 $\mu g.L^{-1}$ each. In parallel, 5 mL of the spiked solution, not exposed to light during the experiment, served as a control to ensure the absence of degradation via other processes (e.g. hydrolysis). In each of the solutions (control + reactor), a mixture of 22 perdeuterated internal surrogates at concentrations of 20 $\mu g.L^{-1}$ was added as a quality control.

The reactor solution was placed in the suntest chamber, which was positioned in a dark room for the duration of the experiment. We collected 25 mL samples after 0, 0.5, 1, 2, 3, 4, 8, 24, 36, 53, 77, 149 and 173 hours of exposure in the suntest.

The pH and the temperature of the reactor were checked at each sampling time. The pH checks ensured compliance with the conditions encountered in a natural environment (water pH $\approx$ 7). Temperature monitoring showed a relatively high temperature (close to 40°C). To ensure that the full decrease in the concentration of micropollutants was due solely to their photodegradation, we also assessed their degradation by hydrolysis and thermolysis, as well as losses by adsorption. To this end, we carried out the same experiments but in the dark, and for the evaluation of thermolysis, in an oven at 40°C.

2.3. Micropollutants analysis

We performed direct injections of water samples in the chromatographic system. The analysis of the micropollutants was performed by ultra-high performance liquid chromatography (UHPLC Nexera 2, Shimadzu) coupled with tandem mass spectrometry (AB Sciex API 4000) (LC-MS/MS). The separation was performed on an ACQUITY UPLC HSS-T3 column (C18, 100 × 2.1 mm × 1.7 µm), preceded by a pre-column of the same phase (5 × 2.1 mm × 1.7 µm). The MS/MS acquisition on a triple quadrupole was performed in positive ionization. The compounds were quantified by internal calibration from a quadratic type calibration line containing the compounds and their associated deuterated derivatives.

This validated analytical technique gave robust micropollutant concentrations, with low limits of quantification (LoQ = 0.1–5 $ng.L^{-1}$) (Table 1). A UHPLC chromatogram of the standard solution including the 36 studied micropollutants in the mobile phase is available in SPM5.

2.4. Data analysis

2.4.1. Determination of the kinetic constant k and half-life $t_{1/2}$

Several studies have shown that photochemical reactions contribute to the breakdown of pesticides and pharmaceuticals in water exposed to solar radiation (Burrows et al., 2002; Fatta-Kassinos et al., 2011). These reactions take place through photolysis, in which a chemical compound is broken down with the energy of light rays. The rate of disappearance is generally expressed using kinetics of order 1 (Equation 1), with the half-life defined by Equation 2, as follows:

$$-\frac{d[MP]}{dt} = k.[MP] \qquad \text{(Eq. 1)} \qquad\qquad t_{1/2} = \frac{Ln\ 2}{k} \qquad \text{(Eq. 2)}$$

where [MP] is the concentration for a micropollutant, *k* is the kinetic constant of direct photolysis, and $t_{1/2}$ is the half-life of the micropollutant.

To determine this kinetic constant *k*, the graph Ln ([MP](t)/[MP_0]) = *f*(*t*) is drawn. The direct coefficient of the linear regression of the data points is the constant *k* (Figure 2). As we will see, the studied micropollutants photodegraded with different kinetics. Some micropollutants were partially photodegraded (atrazine, atenolol and diazepam) after 173 h of exposure, while others completely degraded after only 30 min of exposure (PROP, KETO and AFENO). Thus, the number of data points used to draw the linear regression ranged widely according to the micropollutant (Table 3). For some micropollutants, the LoQ was reached well before 30 minutes. So, the constant *k* was determined with only two concentrations, the initial and the final concentration (LoQ); it is a minimum approximate value for these special cases.

2.4.2. Comparison of $t_{1/2}$ obtained in laboratory and in situ: correction of differences in light intensity

In order to compare the results obtained in laboratory in the present study with those obtained in CW (Mathon et al. 2019), or with results from the literature. (review by Mathon et al. 2016), we compared the light emission spectrum of the lamp used in the laboratory with different solar light spectra measured at noon in summer when the intensity is close to maximum (SPM 4). We considered an average daily light duration of 11 h in summer and 9 h in winter. The light intensity of our experiment was on average 1.4 times greater than the intensity measured in Miami, USA and 3.1 times greater than that measured in the CW of Marguerittes (Mathon et al. 2019).

We developed a method to compare the $t_{1/2}$ obtained in laboratory with values obtained previously with direct photodegradation in the CW of Marguerittes (Hérault, France), according to Mathon et al. (2019). These *in situ* experiments were carried out in flasks immersed at different water depths, containing pure water spiked with micropollutants (also at 10 µg.L^{-1}). We report in Table 3 the $t_{1/2}$ obtained at depth 10 cm. To compare the $t_{1/2}$ measured in laboratory with that measured *in situ*, we normalized the light

intensity measured *in situ* to that controlled in laboratory, by evaluating correction factors, for each hour of exposure in the field. These factors took into account (i) the light intensity (300–400 nm) of the suntest lamp (84 Wm^{-2}) used in the laboratory, which is the reference intensity, and (ii) the light intensity at depth 10 cm in the CW, evaluated by several measurements with a spectroradiometer (obtaining a light intensity by wavelength on the UV range from 290–550 nm) and corrected by continuous measurement with a pyranometer (obtaining a less precise average light intensity over the range 300–1100 nm). This method allows to integrate reduction in light intensity linked to climatic conditions (clouds, fog, etc.) and to the physico-chemical parameters of the water (suspended matter, natural organic matter, etc.).For example, we recorded 14 $W.m^{-2}$ (290–550 nm) with the spectroradiometer during the summer campaign, the first day at noon; at the same time, we recorded 831 $W.m^{-2}$ (300–1100 nm) with the pyranometer. The temporal variation of the light intensity was then evaluated with the pyranometer continuously (every 2 minutes) throughout the *in situ* experiment, to extrapolate a temporal variation with the spectroradiometer. Finally, for *in situ* measurements, we obtained a light intensity over the UV range from 290 nm to 550 nm, and hour by hour. For each period of 1 hour of exposure in the field, we could recalculate how much this represented in equivalent hours of exposure to the suntest lamp (laboratory condition).

2.4.3. Statistical analyses to study the relationships between physico-chemical properties of micropollutants and their photodegradability

The R software was used for the statistical analyses carried out in this study. To classify micropollutants into different classes according to their functional groups and covalent bonds, the Ascending Hierarchical Classification (AHC) according to the Ward criterion was implemented. Ward's method consists of making classes of micropollutants, so that the increase in the inter-class inertia is maximum (Legendre & Legendre, 2012). The distances between the micropollutants are calculated from their respective numbers of functional groups based on the Bray-Curtis dissimilarity (Legendre & Legendre, 2012). A Correspondence Analysis (CoA) (Braak, 1986; Jongman et al., 1995) was then carried out on the same data to project the micropollutants classified into classes and their constitutive functional groups in the same space with reduced dimensions. The CoA grouped certain micropollutants and highlighted their characteristic functional groups. The distribution of the values of the CoA formed a three-dimensional space carrying a significant proportion of the total variability of the data.

Before using the data from $t_{1/2}$ in laboratory or *in situ*, we had to make sure their respective distributions were Normal. The Shapiro-Wilk test was used to assess the correspondence of the distribution of $t_{1/2}$ (less than 50 observed values) with that of the Normal distribution (Shapiro and Wilk, 1965). However, it turned out that the distributions of $t_{1/2}$ were closer to the normal distribution once they had been transformed into decimal logarithms (*p*-values increased from $5.3.10^{-5}$ to $1.3.10^{-4}$ for $t_{1/2}$ in laboratory and from $4.5.10^{-7}$ to $7,1.10^{-3}$ for $t_{1/2}$ *in situ*).

The laboratory and *in situ* $t_{1/2}$ values of the micropollutants composing each of the classes established by the two previous analyses were studied to conclude on significant differences in $t_{1/2}$ between these classes. For this purpose, Kruskal-Wallis tests were carried out to validate a typological effect on $t_{1/2}$; these tests were then supplemented by a Dunn test to identify the differences in $t_{1/2}$ by pairs of classes (Dinno, 2016).

We then considered all chemical functions as well as log K_{ow}, molecular weight and quantum yield (Φ), parameters that could explain the variables for $t_{1/2}$. To identify those most significantly correlated with laboratory and *in situ* $t_{1/2}$, we used the multiple linear regression model:

$$y_i = \beta_0 + \sum_{j=1}^{k} \beta_k x_{ik} + e_i \qquad \text{(Eq. 3)}$$

where k is the number of explanatory variables and i one of the individuals in the observed population, β_0 is a constant, $\beta_{1 \text{ to } k}$ represents the coefficients associated respectively with the k explanatory variables $x_{1 \text{ to } k}$, y_i the variable to be predicted and e_i represents the Gaussian error associated with the model.

Finally, we applied the stepwise regression method (Venables and Ripley, 2002) to select the most influential variables for $t_{1/2}$, among 19 variables: molecular weight, log Φ, log K_{ow} and 16 functional groups weighted with its dissociation energy (see Table 2). A functional group with a high dissociation energy requires a greater supply of energy (here provided by absorbed UV radiation) to be broken, and so will be less sensitive to photodegradation. The stepwise method is based on Akaike's Information Criterion (AIC), which measures the trade-off between the raise of goodness-of-fit with the model complexity.

Table 2. Chemical functions sensitive and refractory to photodegradation (Hammami, 2008) and dissociation energy of their covalent bonds (Blanksby & Ellison, 2003) considered in our multiple linear regression models.

Sensitive functional groups	**Dissociation energy (kcal.mol^{-1})**	**Refractory functional groups**	**Dissociation energy (kcal.mol^{-1})**
Carbonyl (-C=O)	178.1	Primary amine (-NH_2)	85.2
Alkene (-C=C-)	146.7	Secondary amine (-NH-CH_3)	87,0
Nitro (=NO-OH)	70.1	Tertiary amine (-N-$(CH_3)_2$)	90.0
Imine (-CH=N-)	147.0	Hydroxyl (-OH)	92.1
Phenyl (-C_6H_5)	104.0	Ether oxide (-O-)	0.5
Sulfone (O=S=O)	275.0	Chloride (-Cl)	81.0
Phosphinate (-O-P=O)	130.0	Fluoride (-F)	108.3
Oxime (-C=N-O-)	48.0		
Carboxylic acid (OH-C=O)	160.0		

3. Results and discussion

3.1. Kinetic constants of direct photodegradation and classification

From the preliminary experiments (see part 2.2), we checked that the degradation by hydrolysis, thermolysis and the losses by adsorption were negligible (<10%).

Considering a first order kinetics photodegradation, we observed three main micropollutant behaviors, (Figure 1, Table 3). A first group, composed of seven micropollutants, and illustrated with DICLO and SULFA, were fast degraded, with a 90% decrease in the initial concentration in less than 200 minutes (or 3.3 h). The second group, composed of 24 micropollutants, represented by diuron and sotalol, was medium degraded, with a 90% decrease in the initial concentration by around 4000 minutes (or 67 h). Finally, at third group, composed of five micropollutants, represented by atrazine and azithromycin, was slow degraded, with a 90% decrease in the initial concentration of less than 10,000 minutes (or 167 h).

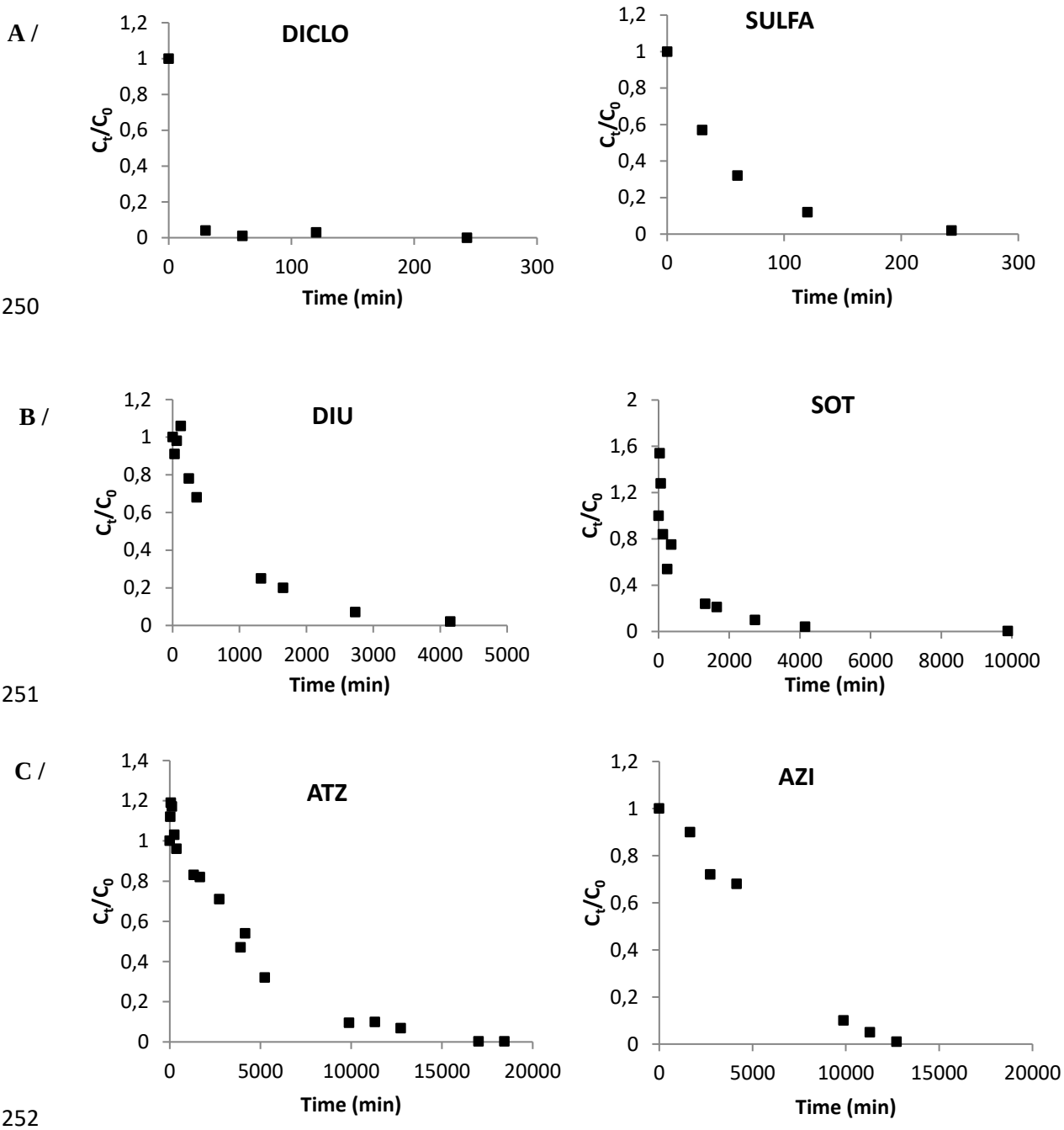

Figure 1. Evolution over time of the concentration of six micropollutants (DICLO, SULFA, DIU, SOT, ATZ and AZI) subjected to exposure in a suntest (lamp power 765 W.m^{-2} with wavelength > 300 nm; [MP]$_0$ =10 µg.L^{-1}) in a reactor containing pure water. A / fast photodegradation, B / medium photodegradation and C / slow photodegradation

From these kinetic curves, we determined the kinetic constants k and $t_{1/2}$ of each micropollutant, as explained in part 2.3.1. These results are reported in Table 3.

3.2. Comparison of $t_{1/2}$ evaluated in laboratory with $t_{1/2}$ in the literature

In a recent review on photodegradability of 13 pharmaceuticals and pesticides, $t_{1/2}$ from the literature were collected and reported and we proposed a classification based on the direct photodegradation

(Mathon et al., 2016). This classification was as follows: a first group, consisting of fast photodegradable micropollutants, with $t_{1/2}$ lower than 8 h, a second group of medium photodegradable micropollutants with $t_{1/2}$ between 8 h and 168 h, and finally a third group of slow photodegradable micropollutants with $t_{1/2}$ greater than 168 h. These groups were defined based on a one-day sun exposure in France. However, according to part 2.4.2, the laboratory suntest irradiation power was on average 3.3 times higher than one-day real sun exposure. To be consistent with the literature, we therefore recalculated the $t_{1/2}$ thresholds measured under laboratory suntest exposure (by dividing them by 3.3): the fast photodegraded micropollutants now have $t_{1/2} < 3.1$ h, those medium photodegraded have $t_{1/2}$ between 3.1 h and 65 h, and those slow photodegraded have $t_{1/2}$ greater than 65 h. These results are presented in Table 3.

In this way, the seven micropollutants classified in the fast group have $t_{1/2}$ between 0.05 h for AFENO and 0.79 h for IMI, the 24 micropollutants in the medium group have $t_{1/2}$ between 5.3 h for TRI and 49.7 h for SMZ, and the five micropollutants classified in the slow group have $t_{1/2}$ between 56 h for ATZ and 118 h for AZI.

The curves $\ln([MP]/[MP]_0) = f(t)$ (Figure 2) do not have the same number of points, with fewer points for micropollutants fast photodegraded (because their concentrations reach <LoQ more quickly). All graphs are available in SPM 1. We consider that a kinetic constants *k* is reliable if it was determined from at least 5 data points (Table 3, 26 values, in white). Otherwise, the k value constitutes a first estimate with higher uncertainty (Table 3, 10 values, in grey).

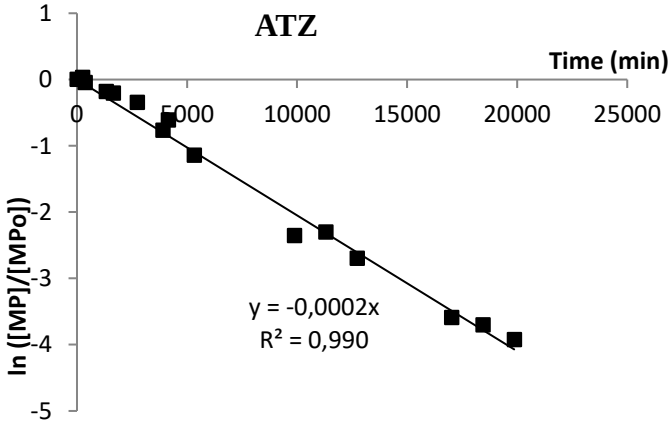

Figure 2. Example of the determination of the photodegradation kinetic constant k for ATZ

Among the 11 micropollutants studied both in laboratory and in the review from Mathon et al. (2016), we finally obtained, as showed in Table 3, the same classification for three micropollutants (DICLO, PROP, ATE), which are well documented in the literature ($n > 30$). By contrast, for seven micropollutants (SMZ, ISO, SOT, DIAZ, DIU, CBZ and MET), we observe some differences. For the first five, there are few data in the literature ($n < 8$), and the classification as proposed in Mathon et *al.*

(2016) was therefore not very robust. For the last two micropollutants, there are much more data in the literature ($n > 14$), but they are dispersed ($t_{1/2}$ between 17 and 12,600 hours for CBZ), which challenges the comparability of $t_{1/2}$ from several different publications. Finally, we note that no $t_{1/2}$ value had been published for ERY before the present laboratory study.

3.3. Comparison of $t_{1/2}$ evaluated in laboratory and $t_{1/2}$ evaluated in situ in a previous study

In Table 3, are listed the $t_{1/2}$ values obtained in laboratory in the present study, the $t_{1/2}$ obtained *in situ* (Mathon et al. 2019), and the $t_{1/2}$ normalized with respect to the light conditions in the laboratory (suntest lamp at 84 $W.m^{-2}$), as explained in part 2.4.2. The ratios $t_{1/2}$ (*in situ*) / $t_{1/2}$ (laboratory) highlight significant differences between micropollutants and depending on the conditions of exposure. We observed $t_{1/2}$ *in situ* in summer on average 8.2 times greater than $t_{1/2}$ in laboratory (with ratios ranging from 0.9 for OFLO to 50 for AFENO). The differences observed are even greater if we consider the winter campaigns with $t_{1/2}$ *in situ* on average 14.2 times greater than $t_{1/2}$ in laboratory (with ratios ranging from 0.4 for ATE to 47 for SULFA).

The differences in $t_{1/2}$ for the same micropollutant can be explained by differences in light intensity between winter and summer, and *in situ* and in laboratory. We then applied correction factors (cf. part 2.4.2.) proportional to the light intensity applied, to allow the comparison of $t_{1/2}$ values obtained in laboratory or *in situ*.

The $t_{1/2}$ values *in situ* with or without correction are compared with the $t_{1/2}$ values obtained in laboratory for 30 micropollutants in common (Table 3). In summer, $t_{1/2}$ (*in situ* corrected) were on average 1.4 times lower than $t_{1/2}$ (laboratory) (with ratios $t_{1/2}$ (*in situ* corrected) / $t_{1/2}$ (laboratory) ranging from 0.11 for OFLO to 2.3 for AFENO). In winter, $t_{1/2}$ (*in situ*) were on average 2.3 times lower than $t_{1/2}$ (laboratory) (with ratios from 0.01 for AFENO to 2 for METRO). This, the use of correction factors based on light intensity clearly improved the correspondence between laboratory and *in situ* data, especially for the micropollutants of the "fast" and "medium" groups.

For the "slow" group, the use of correction factor did not improve the comparability of laboratory and *in situ* data. The difference between averaged light intensity measurement of the present laboratory study and the real light intensity on a CW that fluctuates with time becomes too high. This bias is even higher in winter with a greater variation in light intensity during the day due to weather conditions (clouds, fog, etc.). In addition, the physico-chemical characteristics of real waters of a CW increase the absorption of light intensity and thus the possible bias. It would be interesting to further study the impact of suspended particulate matter, dissolved organic carbon, and chlorophyll A concentrations, and to consider them for the correction factors calculation.

Table 3. The kinetic constants k and $t_{1/2}$ by direct photodegradation of 36 micropollutants determined during the laboratory experiment and in situ for the summer and winter campaigns (CW) and $t_{1/2}$ in the literature described in Mathon et al., 2016 ($t_{1/2}$mean [Min - Max] (number of data)). The number of data points to calculate the kinetic constant k is given, values in grey when number of quantified data < 5. The corrected $t_{1/2}$ values calculated using the approach detailed in part 2.4.2. The micropollutants are classified according to their increasing $t_{1/2}$ in laboratory (fast group blue, medium green and slow red). N.I.A. = no information available.

Micropollutant	*k* (h^{-1})		$t_{(1/2)}$ (h)					
	Laboratory	Number of quantified data to determine *k*	Laboratory	Summer		Winter		In the review from Mathon et al. (2016)
				In situ	*In situ* corrected	*In situ*	*In situ* corrected	
AFENO	13.863	2	0.1	2.5	0.23	0.7	0.08	N.I.A.
KETO	6.931	2	0.1	1.4	0.06	0.7	0.04	N.I.A.
METRO	2.567	4	0.3	2.8	0.18	4.8	0.08	N.I.A.
DICLO	1.873	5	0.4	3.3	0.28	4.3	0.09	4.9 [0.005 - 47] (*n* = 33)
PIRI	1.238	5	0.6	4.2	0.39	14.4	0.37	N.I.A.
SULFA	1.019	5	0.7	15.6	1.4	31.7	0.77	N.I.A.
IMI	0.877	6	0.8	6.1	0.51	19.1	0.53	N.I.A.
TRI	0.131	6	5.3	84.5	9.3	135.9	4.5	N.I.A.
PARA	0.112	4	5.8	119.5	12.8	130.8	4.3	N.I.A.
PROP	0.102	2	6.8	25.1	3.1	90.0	1.6	66 [0.3 - 408] (*n* = 48)
CBZ	0.066	10	10.5	95	10.6	115.5	3.3	2625 [17 - 12600] (n = 35)
ERY	0.066	9	10.5	37.7	4.2	19.7	0.56	No data in literature
OXA	0.061	11	11.4	N.I.A.	N.I.A.	N.I.A.	N.I.A.	N.I.A.
DIU	0.058	10	11.9	119.5	13.4	495.1	16.7	521 [4 - 3192] (n = 8)
CLA	0.050	10	14.0	73.7	8.4	105.0	2.8	N.I.A.
ISO	0.043	12	16.0	105	11.4	277.3	9.7	2.5 [1.4 - 5] (*n* = 4)
ACE	0.040	7	17.2	73.7	8.1	123.8	5.0	N.I.A.
SOT	0.036	11	19.1	85.6	9.4	30.0	1.5	6 (n = 1)
CLIN	0.034	10	20.6	88.9	17.7	182.4	4.0	N.I.A.
OFLO	0.033	5	20.9	19.8	2.3	N.I.A.	N.I.A.	N.I.A.
MET	0.032	4	22.0	84.5	9.4	245.7	4.6	3572 [29 - 11632] (n = 14)
DIM	0.030	9	23.3	95	12.7	990.2	45.7	N.I.A.
AMI	0.029	3	23.7	N.I.A.	N.I.A.	N.I.A.	N.I.A.	N.I.A.
SAL	0.028	10	24.5	108.3	11.9	N.I.A.	N.I.A.	N.I.A.
ASUL	0.023	10	30.6	N.I.A.	N.I.A.	133.3	3.8	N.I.A.
THEO	0.023	11	30.6	126	14.0	154.0	6.5	N.I.A.
ALP	0.020	12	34.2	N.I.A.	N.I.A.	N.I.A.	N.I.A.	N.I.A.
FLUOX	0.015	4	43.4	N.I.A.	N.I.A.	N.I.A.	N.I.A.	N.I.A.
CYC	0.016	7	43.9	83.5	9.8	111.8	2.9	N.I.A.
NORD	0.015	10	46.4	N.I.A.	N.I.A.	N.I.A.	N.I.A.	N.I.A.
SMZ	0.014	18	49.7	130.8	16.2	117.5	2.7	0.08 [0.03 - 0.13] (*n* = 3)
ATZ	0.013	17	56.4	150.7	17.4	288.8	5.5	N.I.A.
ATE	0.012	4	58.6	92.4	10.4	22.1	0.77	1248 [0.1 - 3984] (n = 13)
DIAZ	0.009	10	77.0	115.5	12.5	433.2	9.0	28 [3 - 103] (*n* = 5)
NORF	0.007	4	94.7	N.I.A.	N.I.A.	N.I.A.	N.I.A.	N.I.A.
AZI	0.006	5	118.0	223.6	24.9	N.I.A.	N.I.A.	N.I.A.

3.4. Relationships between the physico-chemical characteristics and structure of the micropollutants and their photodegradability

3.4.1. Understand the direct photodegradation classification with electronic transition

The micropollutants of the three groups were compared to highlight the influence of functional groups and their possible electronic transitions. The two main electronic transitions in photochemistry are the transitions n→π* occurring in the photochemistry of the carbonyl group, and the transition π→π* occurring during the excitation of the double bonds. These electronic transitions lead to an excited state whose lifetime is longer for the n→π* transition than for the π→π* transition (Mousseron, 1969).

The micropollutants of the fast photodegradable group mostly have a nitro (METRO, IMI) or carboxylic acid (AFENO, KETO, DICLO and PIRI) functional group. These chemical groups are characterized by the transition n→π*, which leads to an excited state long enough to promote the photodegradation of the micropollutant. We note the presence in the fast group of SULFA, whereas its degradation product, ASUL, is classified in the medium group. The presence of a carbonyl with an amine group as a substituent of the phenyl instead of an amine alone evidently makes the molecule more resistant to photodegradation.

Among the micropollutants of the slow photodegradable group, AZI does not have a functional group sensitive to photodegradation. In fact, ERY, CLA and CLIN are in the same case, but they belong to the medium photodegradable group. The triazine function, as in ATZ and in SMZ, is a chromophore leading to low quantum yields (Table 1). Thus, despite the presence of -N=N- bonds (with transitions n→π*), these two micropollutants belong to the medium photodegradable group. Finally, the 7-atom heterocycle in DIAZ (slow photodegradable group) and NORD (the least photodegradable compound of the medium group) is unfavourable to photochemical reactions. Thus, the use of electronic transitions does not provide a full understanding of the proposed classification for micropollutants photodegradation. We therefore undertook a statistical analysis to classify the micropollutants according to their chemical functions in order to predict their direct photodegradation.

3.4.2. A new micropollutants classification in 7 classes according to their chemical functions

To go further, we classified the 36 micropollutants according to their chemical functions, by testing the ascending hierarchical classification according to the Ward criterion. The results of this classification are presented in Figure 3.

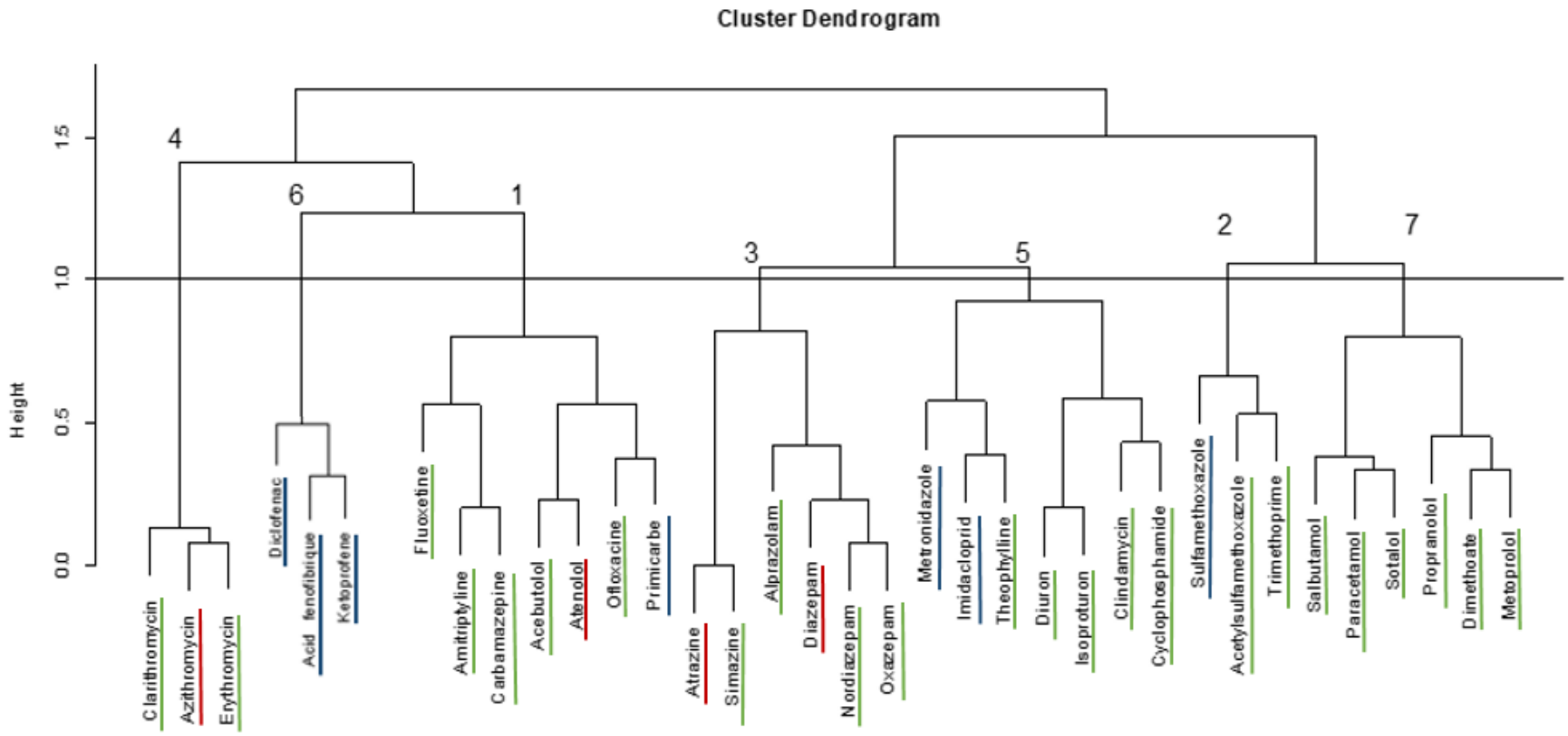

356

357 *Figure 3. Classification of micropollutants into seven classes according to the Bray-Curtis distances on the inventory of functional groups (Table 2) with the*
358 *Ward aggregation criteria. Micropollutants are underlined according to their classification in this study based on the direct photodegradation (fast group*
359 *blue, medium green and slow red)*

A classification was obtained with seven classes of micropollutants according to a rather dichotomous tree structure. Classes 1, 6 and 4 stand apart from the others. Only the distinction of class 4 from the paired classes 1 and 6 is not dichotomous, suggesting a slight gradient effect. Class 4 consists of three micropollutants with the highest molecular weights and no phenyl. The three micropollutants in class 6 have a carboxylic acid function.

As explained in part 2.3.4, we performed a Correspondence Analysis (CoA) to project these seven classes of micropollutants and their various chemical functions in the same space with reduced dimensions (SPM 2).

The distribution of the values retained a three-dimensional space as carrying a significant proportion of the total variability of the data. In this covalent space, class 5 remains fairly central (showing no significant distinction on the basis of its functional groups composition). By contrast, class 4 is clearly distinguished and without great variability among its members (the points being very close together in the covalent space of the CoA). This distinction occurs because this class is composed of high molecular weight micropollutants (>700 $g.mol^{-1}$) with many chemical functions and no phenyl (-C_6H_5). From CoA (SPM2), we observed that class 1 is characterized by a secondary amine function followed by an isopropyl (–NH–CH–(CH3)–CH3). Class 2 is characterized by the presence of the sulfone (O=S=O) and primary amine (–NH2) bonds. Class 3 is characterized by the presence of the chloride (–Cl) and imine bonds (–CH=N–). Classes 4 and 7 are characterized by a strong presence of hydroxyl (–OH) and ether oxide (–O–) bonds. Class 6 is characterized by the carboxylic acid bond (OH–C=O). Finally, Class 5 is fairly central, and it is difficult to highlight specific chemical functions.

Seven classes of micropollutants have been formed according to their functional groups, The correlation between $t_{1/2}$ and these groups was tested in the following part.

3.4.3. Correlation between the $t_{1/2}$ values and the seven classes of micropollutants

Here we are not comparing laboratory and *in situ* data, already discussed in part 3.2. The objective was to identify the classes of micropollutants most sensitive to photodegradation and to conclude on the sensitivity of their functional groups. The graphical representation of log $t_{1/2}$ for the seven classes, distinguishing the $t_{1/2}$ in laboratory from the $t_{1/2}$ *in situ* is illustrated in Figure 4.

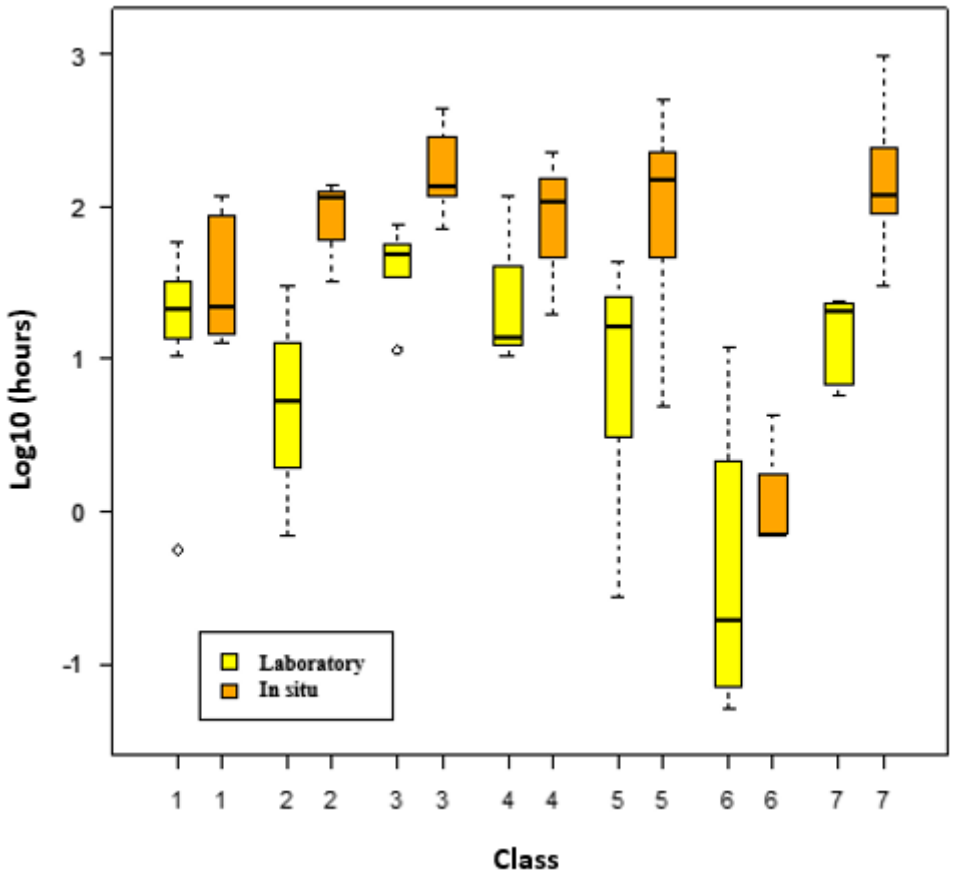

Figure 4. Boxplot representation of $t_{1/2}$ in laboratory (yellow) and $t_{1/2}$ in situ (orange) for the seven classes of micropollutants.

To determine whether the differences in $t_{1/2}$ between each class of micropollutants were significant ($p < 0.05$), Kruskal-Wallis tests were supplemented by Dunn tests (Dinno, 2016). The results are available in SPM 2. Class 6 stands out strongly, with $t_{1/2}$ significantly lower than $t_{1/2}$ in laboratory of classes 1, 3, 4, 5 and 7, and also significantly lower than $t_{1/2}$ *in situ* of classes 2, 3, 4, 5 and 7. Class 3 is characterized by $t_{1/2}$ significantly higher than those of classes 2, 5, 6 and 7 for the laboratory data and those of classes 1 and 6 for the *in situ* data. Finally, the $t_{1/2}$ values of class 7 are significantly higher than those of class 1. To explain the $t_{1/2}$ according to the functional groups, class 6, with the smallest $t_{1/2}$, is characterized by a carboxylic acid function, class 3 is characterized by the chloride and imine functions, and class 7 is characterized by the hydroxyl and ether oxide functions, with the highest $t_{1/2}$. Hence the carboxylic acid function appears to be the most sensitive to photodegradation, while the chloride, imine, hydroxyl and ether functions are the most refractory.

3.4.4. Which chemical properties or functions influence the photodegradability of micropollutants?

In this part, we tested the influence of 19 physico-chemical variables on the $t_{1/2}$. The 19 tested variables are detailed in part 2.4.3. Among the 36 micropollutants, five micropollutants were considered because they do not have quantum yield value available in the literature: ASUL, AZI, FLUOX, NORF and PIRI.

The multiple linear regression model highlighted 11 variables that significantly influenced $t_{1/2}$ laboratory and $t_{1/2}$ *in situ* ($p < 0.05$): molecular weight, log Φ, log K_{ow} and eight covalent bonds listed in Table 2 (OH–C=O, =NO–OH, C=NO–, –O–, –Cl, –OP=O, –CH=N– and –C=C–). Two chemical functions had a significant influence on $t_{1/2}$ with the two datasets: OH–C=O and C=N–O–. Once again, the OH–C=O function induced low $t_{1/2}$ in both cases, confirming the sensitivity of this function to UV radiation (Hammami, 2008). The function C=N–O– is present only in the micropollutant SULFA and contributed to the decrease in laboratory $t_{1/2}$ but to the increase in *in situ* $t_{1/2}$. The =NO–OH function is present in IMI and METRO (class 5) and contributed to a decrease in laboratory $t_{1/2}$. The functions –O– and –CH=N– characteristic of class 3, contributed respectively to the increase and decrease in the $t_{1/2}$ *in situ*. The –Cl function contributed to the increase in the $t_{1/2}$ *in situ*, and is characteristic of class 7. Two new functions are specifically highlighted with this model and contributed to the lower $t_{1/2}$ *in situ* (–O–P=O and –C=C–). These results are consistent with the dissociation energies given in Table 2 and also support the method implemented by combining the dissociation energy of the covalent bonds with the compound photodegradability. This method allowed us to identify the eight most influential functional groups for the direct photodegradation. The molecular weight was evaluated as influential with an increase in $t_{1/2}$ in laboratory only for micropollutants with the highest molecular weights (>700 $g.mol^{-1}$). Log K_{ow} was significantly influential, with an increase in the $t_{1/2}$ *in situ* for decreasing log K_{ow} values. Finally, the quantum yield had a significant influence, with an increase in the $t_{1/2}$ *in situ* for increasing quantum yield values. These observations are summarized in Figure 5. The sign and rank of each variable allow to identify the influence on $t_{1/2}$ (− for a decrease in $t_{1/2}$ and + for an increase in $t_{1/2}$) (see details on the statistical test in SPM2).

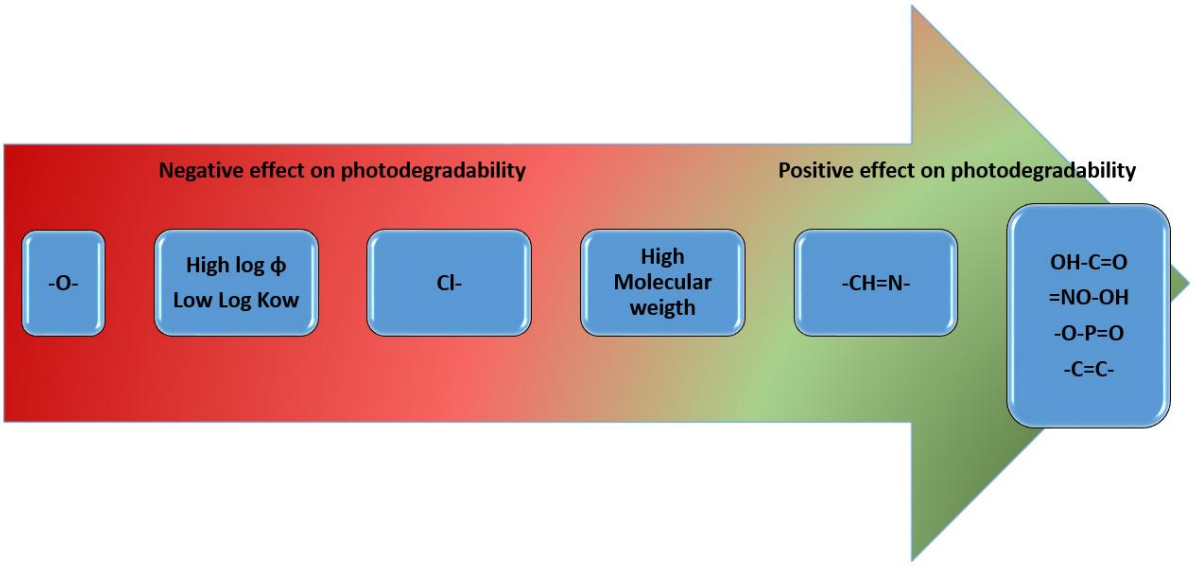

Figure 5. Assessment of the influence of selected chemical properties and chemical functions on the photodegradability of micropollutants

4. Conclusion

This study evaluated the direct photodegradation of 36 organic micropollutants under controlled laboratory conditions. These micropollutants were classified into three groups according to their $t_{1/2}$: seven micropollutants in the fast group ($t_{1/2}$ < 2.5 h), 24 micropollutants in the medium group (2.5 h < $t_{1/2}$ <50 h), and five micropollutants in the slow group ($t_{1/2}$ < 2.5 h). We then compared $t_{1/2}$ determined in controlled laboratory conditions with $t_{1/2}$ previously determined in a CW. The use of correction factors based on precise monitoring of the light intensity proved essential for this comparison. For future studies, in situ or in laboratory, the determination of light intensity and its variation during the experiment is a prerequisite for comparison of $t_{1/2}$ with other data sets. Finally, we statistically tested the relationships between the chemical structure of micropollutants and their $t_{1/2}$. This enabled us to classify the micropollutants into seven classes according to their chemical structures. These tests further highlighted the chemical functions characteristic of micropollutants sensitive to photodegradation (OH–C=O, C=N–O, =N–OH, –CH=N–, –O–P=O, –C=C–) and those with low sensitivity (–O–, –Cl). It would be interesting to test the influence of these chemical functions on a larger set of micropollutants. It would also be interesting to identify the structure of the photodegradation by-products in order to deduce the degradation mechanisms and confirm or not the most sensitive chemical functions.

Acknowledgments

The authors thank the OFB (the French national Office for Biodiversity) for their financial support for this work. We are also grateful to Philippe Bados, Amandine Daval, Thomas Brzokewicz and Clément Crétollier from INRAE for their analytical and technical support.

References

Ben, W., Zhu, B., Yuan, X., Zhang, Y., Yang, M., & Qiang, Z. (2018). Occurrence, removal and risk of organic micropollutants in wastewater treatment plants across China: Comparison of wastewater treatment processes. Water Research, 130, 38-46.

Blanksby S.J. & Ellison G.B. (2003). Bond Dissociation Energies of Organic Molecules. Accounts of Chemical Research 36. 255-263.

Ter Braak. C. J. F. (1986) Canonical Correspondence Analysis: a new eigenvector technique for multivariate direct gradient analysis. Ecology. 67. 1167-1179.

Braun, A. M., Maurette, M. T., & Oliveros, E. (1986). Technologie photochimique. Presses polytechniques romandes.

Brodin, T., Fick, J., Jonsson, M., & Klaminder, J. (2013). Dilute concentrations of a psychiatric drug alter behavior of fish from natural populations. Science, 339(6121), 814-815.

Burrows. H. D.. Santaballa. J. A.. & Steenken. S. (2002). Reaction pathways and mechanisms of photodegradation of pesticides. Journal of photochemistry and photobiology B: Biology. 67(2). 71-108.

Challis. J. K.. Hanson. M. L.. Friesen. K. J.. & Wong. C. S. (2014). A critical assessment of the photodegradation of pharmaceuticals in aquatic environments: defining our current understanding and identifying knowledge gaps. Environmental Science: Processes & Impacts. 16(4). 672-696.

Dinno. A. (2016). Dunn's Test of Multiple Comparisons Using Rank Sums. R package version 1.3.2. http://CRAN.R-project.org/package=dunn.test.

European Commission (2000). Directive 2000/60/EC of the European Parliament and of the Council of 23 October 2000 Establishing a Framework for Community Action in the Field of Water Policy Off J L, 327 (2000), pp. 1-73

European Commission (2015). Commission Implementing Decision (EU) 2015/495 of 20 March 2015 establishing a watch list of substances for Union-wide monitoring in the field of water policy pursuant to Directive 2008/105/EC of the European Parliament and of the Council (notified under document C(2015) 1756. 3 p.

Fatta-Kassinos. D.. Vasquez. M. I. & Kümmerer. K. (2011). Transformation products of pharmaceuticals in surface waters and wastewater formed during photolysis and advanced oxidation processes - Degradation. elucidation of byproducts and assessment of their biological potency. Chemosphere 85. 693-709.

Fent. K.. Weston. A. A.. & Caminada. D. (2006). Ecotoxicology of human pharmaceuticals. Aquatic toxicology. 76(2). 122-159.

Gonzalez-Rey. M.. Tapie. N.. Le Menach. K.. Dévier. M. H.. Budzinski. H.. & Bebianno. M. J. (2015). Occurrence of pharmaceutical compounds and pesticides in aquatic systems. Marine Pollution bulletin. 96 (1). 384-400.

Grandclément, C., Seyssiecq, I., Piram, A., Wong-Wah-Chung, P., Vanot, G., Tiliacos, N., Roche, N., & Doumenq, P. (2017). From the conventional biological wastewater treatment to hybrid processes, the evaluation of organic micropollutant removal: a review. Water research, 111, 297-317.

Hammami. S. (2008). Étude de dégradation des colorants de textile par les procédés d'oxydation avancée. Application à la dépollution des rejets industriels (Doctoral dissertation. Université de Marne la Vallée).

Jongman. R.H.G.. ter Braak. C.J.F.. Van Tongeren. O.F.R. (Eds.). 1995. Data Analysis in Community and Landscape Ecology. Cambridge University. Melbourne.Kolpin.

Legendre. P..& Legendre. L... (2012). Numerical ecology. 3rd English edition. Elsevier Science BV. Amsterdam.

Luo. Y.. Guo. W.. Ngo. H. H.. Nghiem. L. D.. Hai. F. I.. Zhang. J.. Liang. S. & Wang. X. C. (2014). A review on the occurrence of micropollutants in the aquatic environment and their fate and removal during wastewater treatment. Science of the Total Environment. 473. 619-641

Mamy. L.. Patureau. D.. Barriuso. E.. Bedos. C.. Bessac. F.. Louchart. X.. Martin-Laurent. F.. Miège. C. & Benoit. P. (2015). Prediction of the fate of organic compounds in the environment from their molecular properties: a review. Critical Reviews in Environmental Science and Technology. 45(12). 1277-1377.

Mathon, B., Coquery, M., Miège, C., Vandycke, A., & Choubert, J. M. (2019). Influence of water depth and season on the photodegradation of micropollutants in a free-water surface constructed wetland receiving treated wastewater. Chemosphere, 235, 260-270..

Mathon. B.. Choubert. J.-M.. Miège. C.. Coquery. M. (2016). A review of the photodegradability and transformation products of 13 pharmaceuticals and pesticides relevant to sewage polishing treatment. Science of the Total Environment 551-552. 712-724.

Miège. C.. Choubert. J. M.. Ribeiro. L.. Eusèbe. M.. & Coquery. M. (2009).Fate of pharmaceuticals and personal care products in wastewater treatment plants–conception of a database and first results. Environmental Pollution. 157(5). 1721-1726.

Mousseron-Canet, M. & Mani, J.C. (1969). Photochimie et réactions moléculaires. Dunod

Pal. R.. Chakrabarti. K.. Chakraborty. A.. & Chowdhury. A. (2006). Degradation and effects of pesticides on soil microbiological parameters-A review. Int. J. Agric. Res. 1. 240-258.

Reyes Contreras, C., López, D., Leiva, A. M., Domínguez, C., Bayona, J. M., & Vidal, G. (2019). Removal of Organic Micropollutants in Wastewater Treated by Activated Sludge and Constructed Wetlands: A Comparative Study. Water, 11(12), 2515.

Silva, D. B., Cruz-Alcalde, A., Sans, C., Giménez, J., & Esplugas, S. (2019). Performance and kinetic modelling of photolytic and photocatalytic ozonation for enhanced micropollutants removal in municipal wastewaters. Applied Catalysis B: Environmental, 249, 211-217.

Shapiro. S. S.. & Wilk.M. B. (1965). « An analysis of variance test for normality (complete samples) ». Biometrika. vol. 52. no 3-4. p. 591–611.

Tran, N.H., Reinhard, M., Yew-Hoong Gin, K. (2018). Occurrence and fate of emerging contaminants in municipal wastewater treatment plants from different geographical regions-a review, Water Research, Volume 133, 2018, 182-207.

Venables. W. N. & Ripley. B. D. (2002). Modern Applied Statistics with S. Fourth Edition. Springer. New York. ISBN 0-387-95457-0

Verlicchi. P.. Al Aukidy. M.. & Zambello. E. (2012). Occurrence of pharmaceutical compounds in urban wastewater: removal. mass load and environmental risk after a secondary treatment—a review. Science of the total environment. 429. 123-155.

Zepp. R. G. (1987). Environmental photoprocesses involving natural organic matter. Environmental Research Laboratory. Office of Research and Development. US Environmental Protection Agency.